

Some measurements of the short term variability of r_0

L. William Bradford & Lewis C. Roberts, Jr.

The Boeing Company, 535 Lipoa Pkwy., Suite 200, Kihei, HI 96753

lawrence.w.bradford@boeing.com, lewis.c.roberts@boeing.com

ABSTRACT

We present measurements of r_0 collected with the Visible Imager: the science camera for the AEOS telescope’s adaptive optics system. Sequences of long exposure images (0.5 sec – 2.0 sec) give r_0 on a timescale of a few minutes. Significant variability of measured r_0 is found. The implications of this for modeling and simulation are discussed.

Subject headings: atmospheric effects, site testing

1. Introduction

The variations in image quality or “seeing” observable in images is primarily due to fluctuations in the index of refraction of the air through which the light propagates. These index of refraction fluctuations are due to fluctuations in air temperature arising from turbulent motions. These turbulent motions tend to be on scales smaller than the grosser motions of the winds and are commonly held to follow the scaling law of (Kolmogorov 1941), although reports of non-Kolmogorov behavior also appear in the literature (Nicholls et al. 1995; Beyer et al. 2003).

For the observational astronomer, the implications of atmospheric turbulence were evident in any long exposure image of a point source: the image was not the Airy pattern described by diffraction theory (Born & Wolf 1999), but a rather more extended blur of roughly Gaussian shape (King 1971). The measure of the “seeing” was the full width across the image where it was one-half of the maximum intensity (FWHM). The better the seeing, the smaller the FWHM. Armed with the analysis tools developed by Tatarskii and his colleagues (Tatarski 1961), Fried advanced the statistical models of the effects of turbulence on light propagating down through the atmosphere (Fried 1965, 1966). Out of this work came the identification of a particular spatial coherence length scale r_0 . This scale could be used to predict the influence of the path-integral of the fluctuations of index of refraction on both

long and short exposure images. A later analysis (Korff 1973) discussed the relation of the FWHM to r_0 . Later, (Sarazin & Roddier 1990) cited a numerical estimation that led to the oft-used result

$$FWHM = \frac{C\lambda}{r_0}, \quad (1)$$

where $C = 0.98$. For convenience we have set $C = 1$. We feel that measurement uncertainty contributes more error than this small difference in a coefficient. We therefore have a means of obtaining r_0 from long exposure images. By examination of images with different exposure times, we feel that exposures of 0.5 s or more suffice to produce an image that yields an easily estimated FWHM, assuming aberrations other than the atmosphere are small.

Fried’s analysis also showed that one could obtain estimates of r_0 from short exposure images. Schneiderman & Karo (1978) used speckle interferometry measurements at the Maui Space Surveillance System (MSSS) on Haleakala to estimate r_0 . Other methods, such as the modulation transfer method of Walters & Kunkel (1981), also could make relatively rapid measurements. However, the method of interest here is that of differential angle-of-arrival, which can be used to make rapid sequences of measurements of the differences in wavefront slope between pairs of apertures (Fried 1975). This method was first demonstrated at MSSS (Greenwood et al. 1976), but is more widely known from the work at the European Southern Observatory (ESO) (Sarazin & Roddier 1990; Lopez & Sarazin 1993).

2. Data Collection and Processing

The Visible Imager is the current science camera for the Advanced Electro-Optical System (AEOS) telescope’s adaptive optics (AO) system (Roberts & Neyman 2002). In 2004–2006, we collected about 10000 images of bright ($M_v \approx 2$ to $M_v \approx 4$) stars using a filter centered at 850nm. Observed stars were within 20° of zenith. Data were collected with exposure times such that images did not saturate, with no exposures shorter than 0.5 s or longer than 2 s. The images were collected open loop (tip/tilt and AO control loops off), so images needed to be centered in the $10''$ field of view. Typically a set of 100-120 images were taken successively. If time was available, more than one set of data per night was collected, but this did not occur very often.

Images were automatically processed using a MATLAB script. The first step of the processing was to debias, dark subtract and flat field the images. Then the the image peak was located and the FWHM was measured by radially averaging energy around the peak.

The processing is robust and will give an estimate of FWHM in even poor seeing. Values of r_0 are computed for each FWHM and time series, power spectra, and histograms of the data were computed.

We found it useful to make animations of the images for diagnostic purposes. Thus, when images of double stars were found, that data was not used at this time. Similarly when the AEOS active mirror figure model was not regenerated over a period of time, the image degradation was apparent from the measured r_0 s, which fell to about one half of previous and subsequent values. From this data, we have selected 3209 one-second exposures, and 2495 two-second exposures.

3. Analysis of the Long Exposure Data

Figure 1 show the histograms of r_0 for each set of exposure times. The solid line corresponds to the two second exposure and the dashed line to the one second exposure. The difference in the two data sets is quite startling and one would not expect that taking a longer exposures of stars would lead to larger FWHM and hence smaller r_0 . However, this difference seems most likely to reflect the human-in-the-loop of these measurements. If we are examining a star image at a low r_0 , the image intensity is more spread out, hence lowering the peak value. Since we have elected to keep the peak value in a certain range, we will then increase the exposure time. For cases where the FWHM is smaller, the peak is higher, and we elect to use the shorter exposure time. Another selection effect is that when r_0 is very low, it becomes more difficult to keep the image centered, and data simply may not be collected.

The histograms in Figure 1 are interesting, but we are interested in the variability on short time scales, not statistical means of accumulated data. We therefore show some example time series of r_0 for poor, moderate and excellent seeing conditions. As noted in (Bradley et al. 2006), the median r_0 at Haleakala, based on DNSM measurements is 14.7 cm. Figure 2 has a median r_0 value of 5.8 cm. It displays relatively little variability from that median, with a low of about 3.5 cm and a high of 8 cm. Figure 3 has a median r_0 value of 14.6 cm, and displays somewhat more variability with a low of 5 cm and a high of 29 cm. Figure 4 has a median r_0 value of 26.5 cm and significant variability with a low of 15 cm and a high of 41 cm.

Although not true in every instance, we find that when r_0 is low, the measured values tend to stay low. When r_0 is high, there can be significant variability. This variability does not seem to represent noise in the measurement however. Examination of the time series

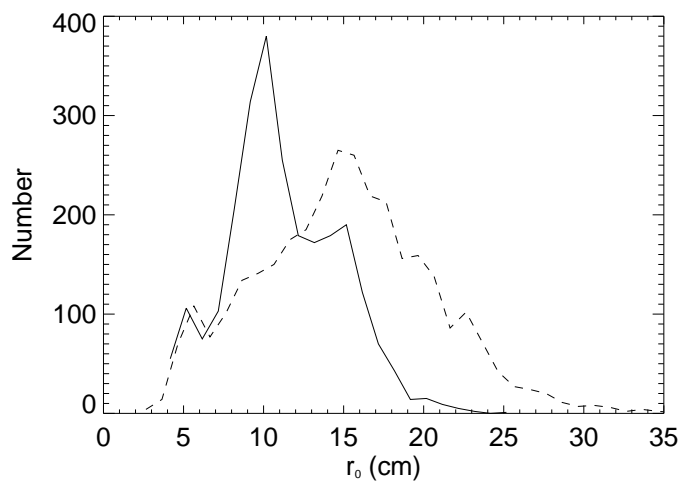


Fig. 1.— Summary histogram of r_0 s computed from one second(dashed line) and two second (solid line) exposures using the Visible Imager. The difference between the histograms represents a selection effect rather than some deviation from theory, as discussed in the text. Data has been corrected to a wavelength of $0.5\mu\text{m}$ and zenith.

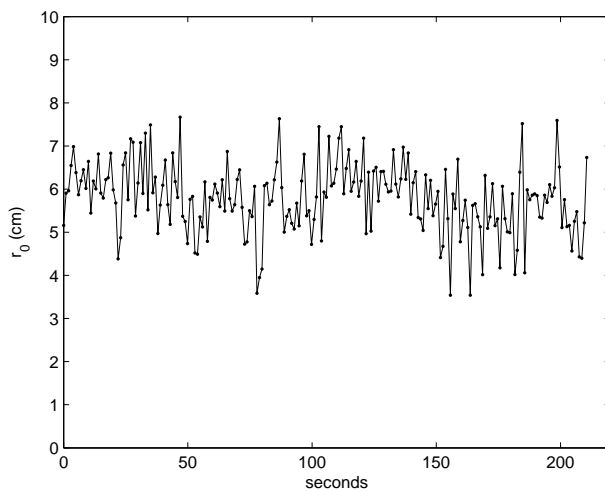


Fig. 2.— Sequence of r_0 s computed from one second exposures using the AEOS Visible Imager science camera. The seeing shown here is some of the worst seen in our data. Relatively little variability in r_0 is seen. The median $r_0=5.8$ cm. Data has been corrected to a wavelength of $0.5\mu\text{m}$ and zenith.

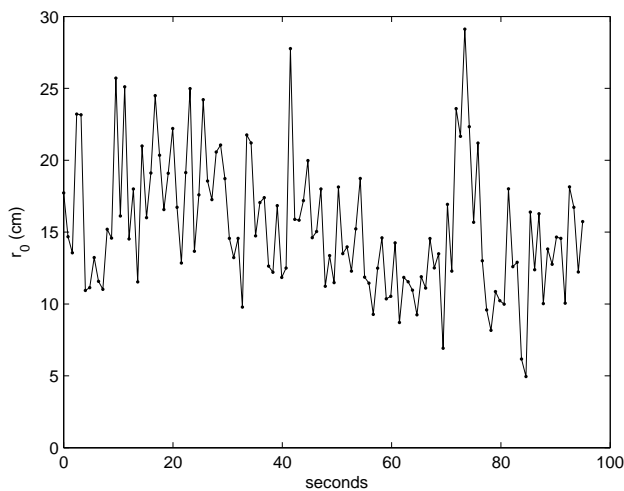


Fig. 3.— Sequence of r_0 s computed from 0.8 second exposures using the AEOS Visible Imager science camera. The median r_0 is 14.6 cm, which is very close to the site median as reported in (Bradley et al. 2006). Data has been corrected to a wavelength of $0.5\mu\text{m}$ and zenith. Note change in vertical scale from previous figure.

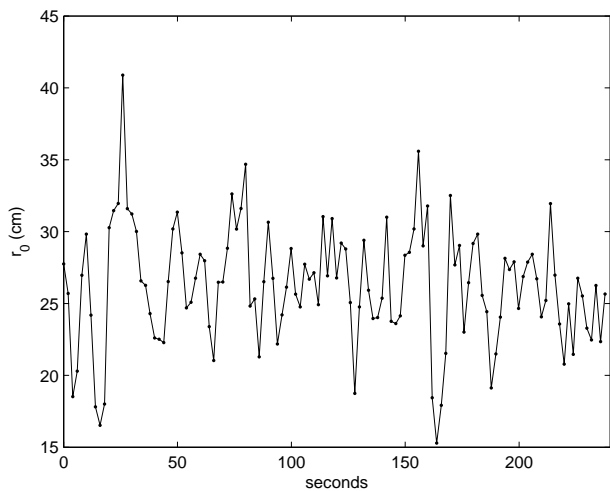


Fig. 4.— Sequence of r_0 s computed from two second exposures using the AEOS Visible Imager science camera. The seeing shown here is some of the best seen in our data. Significant variability is seen in the data set which has a median $r_0=26.5$ cm. Data has been corrected to a wavelength of $0.5\mu\text{m}$ and zenith. Note change in vertical scale from previous figures.

shows that while there are instances of significant swings in value from one measurement to the next, there are many instances of trends in the measurements. See for example, the first dozen or so points in Figure 4. We feel that the measurements reflect true variations in the seeing on the time scale of seconds.

To obtain a better idea of the frame to frame variability of r_0 , we constructed the histogram shown in Figure 5. The histogram is of the change in r_0 from one frame to the next. There are separate histograms for the 1 s and 2 s exposures. The 1 s exposure data is the dashed line, and the 2 s exposure data is the solid line. The histograms show that no change or small changes are the most likely. The larger width of the one second data reflects the greater variability of that data, which had a larger median r_0 . The other reason for the narrowing of the two second data is that the longer exposure will average out some of the larger differences that might occur in one second exposures.

Another way of looking at the variability is shown in Figures 6 and 7. Here we have plotted change in r_0 from one frame to the next on the horizontal axis, and the value of r_0 for the first of the two frames on the vertical axis. Number of measurements for that r_0 is represented by the intensity. There are many values of r_0 between 10 cm and 20 cm, fewer at higher and lower values. Also more values of the subsequent r_0 measurement are close to the first measurement. Therefore the density of points is high. As the difference in r_0 increases, fewer points are to be found. There is also a bias in that there is a limit on the amount of negative change in r_0 because r_0 cannot be less than zero. The differences between the two figures again tend to represent a selection effect. The two second values tend to have lower r_0 as discussed above. Structure within the plots (especially in the two second data) probably represents sampling statistics. More data would improve the utility of the plot.

4. Analysis of the Wavefront Sensor Data

We now show that significant variability exists on much shorter time scales. Using the AEOS AO System’s Shack-Hartmann wavefront sensor, we can record wavefront slopes at rates of 1 KHz, for up to 4096 frames. This slope data can then be processed to yield r_0 using differential angle of arrival methods. (Figures 8–9), which show a measurement of r_0 made using differential angle of arrival measurements with the wavefront sensor.

As noted in the captions, this data is actually rather noise free, when examined closely. This comes about because each r_0 measurement consists of many thousands of measurements of the difference in angle of arrival between pairs of subapertures. This tends to make the

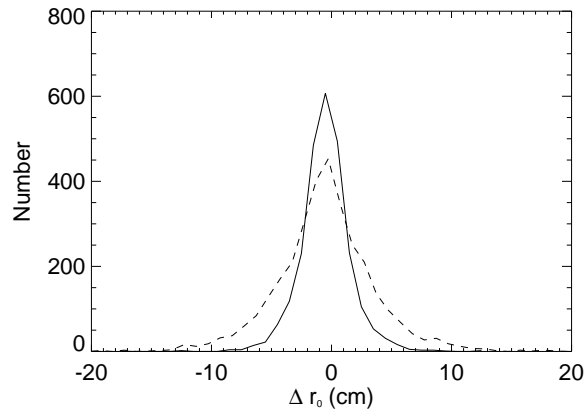


Fig. 5.— Histograms of changes in value of r_0 from one measurement to the next for one second exposures (dashed line) and two second exposures (solid line). Differences between the two figures reflect the selection effect discussed earlier (two second data is more likely to be smaller r_0) and effect of changes being averaged in longer exposures. Data has been corrected to a wavelength of $0.5\mu\text{m}$ and zenith.

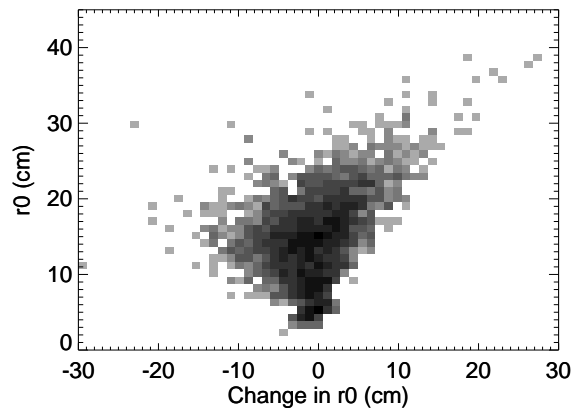


Fig. 6.— Change in r_0 between a one second measurement and its successor versus the value of r_0 for the first measurement. Color represents the number of data points plotted. The data show that more variability in r_0 is seen with larger values of r_0 , while low values of r_0 are less likely to change significantly. A skew toward positive changes in r_0 results from the data being bounded by $r_0=0$ cm. Data has been corrected to a wavelength of $0.5\mu\text{m}$ and zenith.

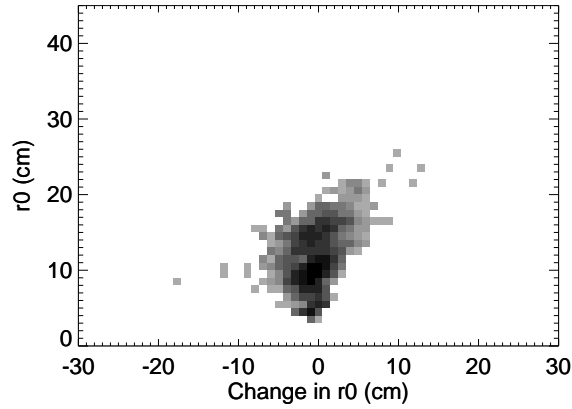


Fig. 7.— Change in r_0 between a two second measurement and its successor versus the value of r_0 for the first measurement. Color represents the number of data points plotted. Comments from figure 6 apply, but there is less variation seen here because the data has a lower median r_0 than the one second data. Data has been corrected to a wavelength of $0.5\mu\text{m}$ and zenith.

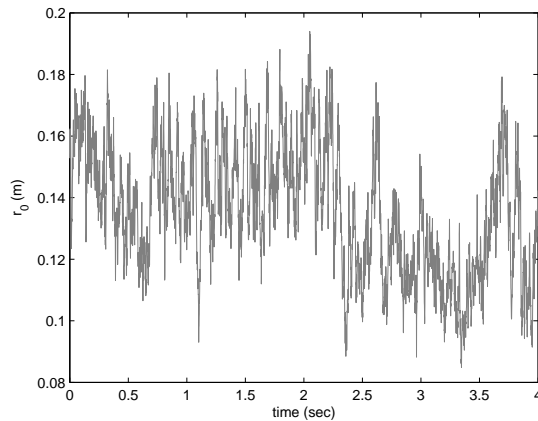


Fig. 8.— A set of r_0 derived from AEOS wave front sensor slope measurements processed by a differential angle-of-arrival code. The sensor frame rate was 1 KHz. Although the data looks noisy at this scale, that perception changes with an increase in resolution.

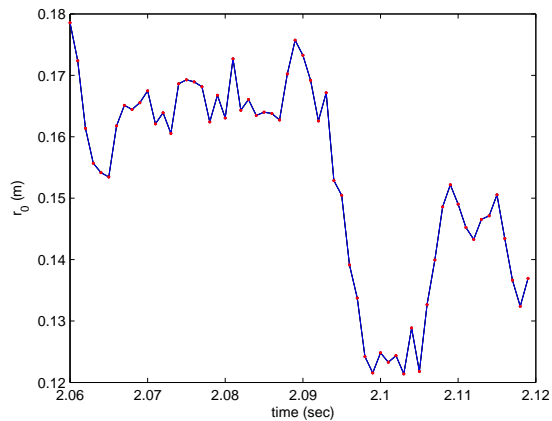


Fig. 9.— A section of r_0 derived from the previous figure. Seen at greater resolution, the noise from measurement to measurement is not large. Even at these short time scales, significant variability exists. Note trends in values and low noise. The low noise reflects the large number of differential angle of arrival pairs used to calculate r_0 .

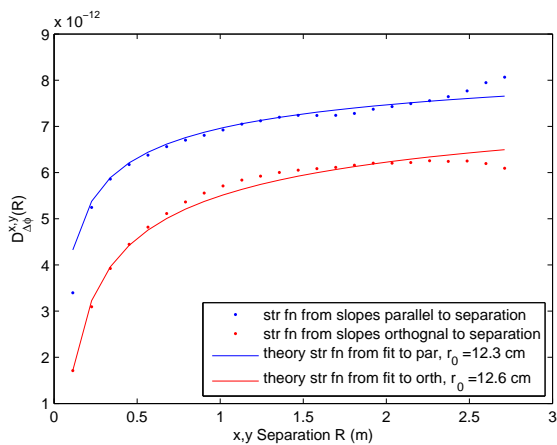


Fig. 10.— Structure functions computed using Roddier and Sarazin formulae, with best fit to theoretical function of r_0 . Structure functions are computed using entire data set.

measurement very robust, particularly for smaller separations, which are most critical to determining the shape of the structure function, since at larger separations, the function is relatively flat. For most differential image motion devices which have perhaps two to four apertures, it is necessary to apply the ergodic hypothesis, and use a time series of differential angle-of-arrival measurements to get a statistically reasonable sample. Here we exploit the spatial ensemble of measurements to get a good value at each measurement time. This means, among other things, that we do not have to assume temporal stationarity of the atmosphere over the entire set of measurements.

We show an example of the structure function for the wavefront sensor data shown. The fit of data to theoretical curves is quite good. The behavior at larger separations could be due to sparsity of data or even outer scale effects.

5. Conclusions and Implications

We have found that r_0 can vary significantly over a period of seconds to minutes. To be sure, this is not a new result. Some of the data described in Walters & Bradford (1997) contained measurements of r_0 at a relatively fine temporal resolution with some data sets, particularly at good seeing sites, showing similar large jumps.

However, our analysis of the statistics of changes in r_0 from one measurement to the next adds to the knowledge base of r_0 variability.

This variability on millisecond time scales is of more interest to the optical scientist than the astronomer. Laser tracking and high speed imaging, such as are done at MSSS may find it helpful to understand that r_0 does vary at this high rate. For imaging purposes, an independent measure of the point-spread-function obtained from data similar to that used to calculate the r_0 would be useful for deconvolution.

How might this information be useful to analysts modeling performance of telescopes? There are two factors that must be accounted for: the time variability and the range of variability of r_0 . We have seen that when values of r_0 are low, the range of r_0 variability within our measurement time intervals is usually low, but when r_0 is high, the range of variation can be larger. It should be noted, however, that for the very short exposures of the wavefront sensor data, we should expect that there is significantly more “bunching” of the data, since it is unlikely that there will be changes as large as those seen on second time scales on millisecond time scales.

Using site data, a modeler could establish a range of r_0 for various conditions (for

example choosing data sets with median values near the 25th percentile, the median and the 75th percentile of the site's r_0 distribution). Then one would compute power spectra for each of these time series. Where more than one time series is available for an r_0 group, the averages of those power spectra can be used as a model power spectra. These model power spectra can then be used to compute time series of r_0 for simulations.

The values of r_0 then determine the cumulative strength of phase screens used by the modeler. Generally one needs to collect somewhat longer sequences of data than we currently have to obtain better statistics, and to estimate probabilities that significant changes will occur over a given time span.

Because we have used the entire telescope to form a single image, our time series of long exposure r_0 measurements does not estimate what variability exists over an aperture, which might be of interest to those modeling effects on much larger telescopes. However, our wavefront sensor measurements can address this, as we shall show in future work.

This research was funded by the Air Force Office of Scientific Research under contracts F29601-00-D-0204 and FA9451-05-C-0257.

REFERENCES

- Beyer, J. T., Roggemann, M. C., Otten, L. J., Schulz, T. J., Havens, T. C., & Brown, W. W. 2003, *Appl. Opt.* 42, 908
- Born, M. & Wolf, E. 1999, *Principles of Optics*, (Cambridge, UK: Cambridge University Press)
- Bradley, E.S., Roberts, Jr., L.C., Bradford, L.W., Skinner, M.A., Nahrstedt, D.A., Waterson, M.F. & Kuhn, J.R. 2006. *PASP*, 118, 172
- Fried, D.L. 1965, *J. Opt. Soc. Am.*, 55, 1427
- Fried, D.L. 1966, *J. Opt. Soc. Am.*, 56, 1372
- Fried, D.L. 1975, *Radio Science*, 10, 71
- Greenwood, D., et al. 1976, Technical Report (RADC-TR-75-295, Rome Air Development Center)
- King, I.R. 1971, *PASP*, 83, 199

- Kolmogorov, A.N. 1941, Dokl. Akad. Nauk. SSSR, 30, 9
- Korff, D. 1973, J. Opt. Soc. Am., 63, 971
- Kuhn, J.R., Waterson, M., Northcott, M., Maberry, M., & Tokunaga, A. 1999, in Proceedings of the AMOS Conference, (Kihei, HI: Maui Economic Development Board), 85
- Lopez, B. & Sarazin, M. 1993, A&A, 276, 320
- Nicholls, T. W., Boreman, G. D., & Dainty, J. C. 1995, Opt. Lett. 20, 2460
- Roberts, Jr., L.C. & Neyman, C.R. 2002, PASP, 114, 1260
- Sarazin, M. & Roddier, F. 1990, A&A, 227, 294
- Schneiderman, A. M., & Karo, D. P. 1978, J. Opt. Soc. Am. 68, 348
- Taylor, G.I., 1938, Proc. R. Soc. London, Ser. A, 164, 476
- Tatarski, V.I. 1961, Wave Propagation in a Turbulent Medium (New York, NY: Dover Press)
- Walters D. L. & Kunkel, K. E. 1981, J. Opt. Soc. Am., 71, 397
- Walters, D.L., & Bradford, L. W. 1997, Appl. Opt, 36, 7876